Self-Similar Dynamics of Large Polymer Rings: A Neutron Spin Echo Study

M. Kruteva,[1] M. Monkenbusch,[1] J. Allgaier,[1] O. Holderer,[2] S. Pasini,[2] I. Hoffmann,[3] and D. Richter[1]
[1]Forschungszentrum Jülich GmbH, Jülich Centre for Neutron Science (JCNS), 52425 Jülich, Germany
[2]Forschungszentrum Jülich GmbH, Jülich Centre for Neutron Science at MLZ, Lichtenbergstraße 1, 85748 Garching, Germany
[3]Institut Laue-Langevin (ILL), 71 avenue des Martyrs, 38000 Grenoble, France

(Received 15 May 2020; accepted 29 September 2020; published 1 December 2020)

This work clarifies the self-similar dynamics of large polymer rings using pulsed-field gradient nuclear magnetic resonance and neutron spin echo spectroscopy. We find center of mass diffusion taking place in three dynamic regimes starting (i) with a strongly subdiffusive domain $\langle r^2(t)\rangle_{\mathrm{com}} \sim t^{\alpha}$ $(0.4 \leq \alpha \leq 0.65)$; (ii) a second subdiffusive region $\langle r^2(t)\rangle_{\mathrm{com}} \sim t^{0.75}$ that (iii) finally crosses over to Fickian diffusion. While the $t^{0.75}$ range previously has been found in simulations and was predicted by theory, we attribute the first to the effect of cooperative dynamics resulting from the correlation hole potential. The internal dynamics at scales below the elementary loop size is well described by ring Rouse motion. At larger scales the dynamics is self-similar and follows very well the predictions of the scaling models with preference for the self-consistent fractal loopy globule model.

DOI: 10.1103/PhysRevLett.125.238004

Polymer melt dynamics is characterized by the fascinating topological interchain interactions that dominate their dynamical behavior. For linear chains topological interactions lead to tube formation that constrains lateral chain motion—via its ends a given chain creeps out of the tubelike constraints imposed by the surrounding chains in the celebrated reptation process [1,2]. Because of the absence of chain ends, caused by their loop topology, polymer rings cannot undergo reptation and exhibit distinctly different static and dynamic properties. The ring topology impacts not only the ring conformation but also pertains to the different role of interactions with the surrounding chains. The related phenomena are not only of fundamental interest, but also are highly relevant, e.g., for a mechanistic understanding of cyclic DNA in chromatin folding in nucleosomes providing thereby easy access to genetic information [3]. This Letter aims at the microscopic experimental evaluation of the initial diffusion and internal dynamics of large ring molecules and its comparison with relevant theories and simulations.

Early work considered the conformation and motion of polymer rings through an array of fixed obstacles. The double folded lattice animal (DFLA) model [4] propounded an analogy to randomly branched polymer—the lattice tree, where relaxation occurs by retraction of double folded strands leading to a terminal relaxation time $\tau_d \sim N^3$ with N the number of monomers, fractal dimension of $d_f = 4$, and a center of mass (com) diffusion $D \sim N^{-2}$. Later on the model was refined correcting the terminal time to $\tau_d \sim N^{2.5}$ [5].

Grosberg *et al.* [6] dismissed the unrealistic limiting fractal dimension of the DFLA model and considered a skeleton lattice tree that branches randomly at an entanglement spacing $d_{\mathrm{tube}} = lN_{e,0}^{1/2}$ where $N_{e,0}$ corresponds to the length of an entanglement strand N_e in the linear counterpart and l is the monomer length. From free energy contemplations the fractal dimension of the backbone or trunk of the lattice tree was evaluated to $d_p = 5/3$, the statistics of a self-avoiding random walk. For the dynamics of this self-similar structure, Grosberg derived $\tau_d \approx \tau_e(N/N_{e,0})^{2.56}$, where τ_e is the entanglement time. Finally in 2016 Rubinstein [7] developed the self-consistent fractal loopy globule (FLG) model that also leads to a limiting fractal dimension of $d_f = 3$. The model is based on the conjecture that the overlap criterion [8,9] in the packing model for entanglements [10] also governs the rule for overlapping loops in polymer rings. Larger overlaps are forbidden by topological constraints. The constant overlap O_{KN} of loops is conjectured to occur in a self-similar way over a wide range of length scales from an entanglement length $N_e \cong N_{e,0}$ or elementary loop size up to ring size R.

In order to discuss the dynamics of such rings in a melt, it is important to note that in a melt of rings the topological constraints are diluting with progressing time, because with time loops of increasing sizes are relaxed and cease to be obstacles in a similar way as tube dilation occurs, e.g., in polydisperse linear melts [11,12]. The timescale is set by the time a loop of a given size has traveled over its own size defining thereby the effective time dependent tube diameter $d(g,t) = \langle r_e^2(g)\rangle^{1/2} = \langle \Delta r_{\mathrm{com}}^2(g,t)\rangle^{1/2}$ (r_e: end to end distance of a loop containing g monomers; d: characteristic loop size or effective tube diameter). The equation holds for complete tube dilation, which is supported by MD simulations; with $d_f = 3$: $d(t) \cong d_{\mathrm{tube}}[g(t)/N_{e,0}]^{1/3}$, and $d(\tau_e) = d_{\mathrm{tube}}$. The FLG assuming complete tube dilation is also termed a self-consistent FLG model and leads to

$\tau_d = \tau_e(N/N_{e,0})^{2+1/d_f}$. For the com diffusion constant the model predicts $D_{\rm com} \cong R_g^2/\tau_d = D_{R,e}[N/N_{e,0}]^{-2+1/d_f}$ with $D_{R,e} = d_0^2/\tau_e$, the Rouse diffusion coefficient of one elementary loop. Without tube dilation [13] (so-called naive FLG model) the terminal times are $\tau_d \cong \tau_e[N/N_{e,0}]^{2+d_p/d_f}$ and the diffusion becomes $D_{\rm com} \cong D_e[N/N_{e,0}]^{-2+(2-d_p)/d_f}$. We remark: self-similar relaxation implies that any section of the ring larger than $N_{e,0}$ relaxes in the same way as the whole ring; thus, the FLG model for a mode p leads to $\tau_p = \tau_e[N/(pN_{e,0})]^{2+1/d_f}$ and correspondingly for the other models $\tau_p \cong \tau_e[N/pN_{e,0}]^{2+d_p/d_f}$. Given this property, we embrace the scaling models also as spectral models and the exponents as spectral exponents. On the basis of the experimentally [14] determined fractal ring dimensions $d_f = 1/\nu$ with small variations owed to slightly different ν, for the spectral exponents the models predict: FLG: 2.45; DFLA: 2.5; Grosberg: 2.75; naive FLG: 2.9.

Aside from theoretical modeling a significant amount of MD simulations is available [15–20]. Using coarse grained models, the largest MD-simulation effort so far is due to Halverson *et al.* [15], where rings up to 57 N_e equivalents were simulated. In some disagreement to the predictions of the scaling models, for ring diffusion they found $D \sim N^{-2.3}$. Furthermore, the N dependencies of ring and linear counterparts were found to be equal, with the prefactor for ring diffusion about 7 times larger than that for linear chains. In agreement with theoretical predictions, the simulation revealed subdiffusive behavior $D \sim t^{0.75}$ up to times and distances of about to 2 to 3 times R_g^2 [5,21]. The internal rearrangements of longer rings were found to occur much faster than the time it takes to diffuse over their own size. But on the other hand the $t^{1/4}$ regime in the segment self-correlation function extends to 2 to 3 times of R_g^2; there exists no second $t^{1/2}$ regime as for linear chains [2]. Atomistic simulations on large poly(ethylene oxide) (PEO) rings corresponding to the 10 and 20 K samples [17] were analyzed in terms of Rouse modes that were found to provide an orthogonal basis also for rings. The Rouse spectrum $\tau_p \sim p^{-2}$ was found not to change even for the largest ring, while the Rouse amplitudes were diminishing for low p. Very recently Wong and Choi [19] in terms of an united atom model presented MD simulation for polyethylene (PE) rings in connection with a polymer reference interaction site model, where aside from normal Fickian diffusion a short time regime with $\langle r_{\rm com}^2(t)\rangle \sim t^{0.42}$ was observed.

We studied the internal motions and the connected short time diffusion properties of very large PEO rings of sizes up to 44 entanglement equivalents of the corresponding linear chain. We find three dynamic regimes for the center of mass diffusion and show that the internal dynamics follows the concept of self-similar motion as proposed in the spectral models, in particular Rubinstein's FLG model [7].

The procedure for the synthesis and characterization of the large PEO rings is described in [14]. Molecular weights are summarized in Table I. Size exclusion chromatography also proved the absence of higher molecular weight condensation products in all samples. The conformation of all rings was studied by small angle neutron scattering (SANS) [14] and conformational parameters are also presented in Table I.

We measured the long range diffusion for each ring with pulsed-field gradient nuclear magnetic resonance (PFG NMR) using a Varian 600 MHz system for the larger rings ($R40$, $R100$) and Minispec 20 MHz from Bruker for smaller rings ($R10$, $R20$) at 413 K. The inset in Fig. 1 displays the NMR diffusion data at 413 K as a function of ring size in a double logarithmic plot revealing $D_{\rm com} \sim N^{-2.2}$ in good agreement with Halverson's MD simulations [15]. Figure 1 (inset) includes also diffusion data from linear PEO chains at 413 K [23]. We find the slopes to be slightly different (−2.3 instead of −2.2) and the diffusivities differ by about a factor of 10 in fair agreement with simulations [15]. For the neutron spin echo (NSE) experiments samples containing 10% protonated rings in the corresponding deuterated matrix were prepared. With these samples the NSE experiments addressed the intraring pair correlation function $S(q,t)$. The measurements were

TABLE I. Achieved ring polymer materials; number of entanglement equivalents $Z_{e,0} = M_w/M_{e,0}(M_{e,0} = 1980$ g/mol) [14]; radii of gyration R_g; inverse fractal ring dimensions $\nu = 1/d_f$; subdiffusivity exponent α for the initial com diffusion; scaling exponent μ describing the internal ring dynamics; crossover mean squared displacements (MSD's) of the com diffusion. Some dynamic results on the smaller $R10$ and $R20$ rings were already published recently [22].

Ring	M_w	$Z_{e,0}$	R_g/Å	ν	α	μ	$\langle r_2^2\rangle$/Å^2	$\langle r_1^2\rangle$/Å^2
*hR*100	87300	44	49.8[a]		0.41(1)	2.4(1)	6300	2300
*dR*100	96000	⋯	49.8[a]	0.430				
*hR*40	44000	22	38.5		0.54(4)	2.4(1)	3885	1424
*dR*40	38600	⋯	35.4	0.448				
*hR*20	21000	10			0.53(5)	2.6(0)	1924	740
*dR*20	21900	⋯	27.8	0.451				
*hR*10	10100	5			0.65(4)	5.0(8)	1200	440
*dR*10	11200	⋯	21.4	0.460				

[a]The molecular weights of the $R100$ are slightly higher than quoted in Ref. [14] (new synthesis); the R_g were corrected using $R_g^2 \sim N^{0.78}$

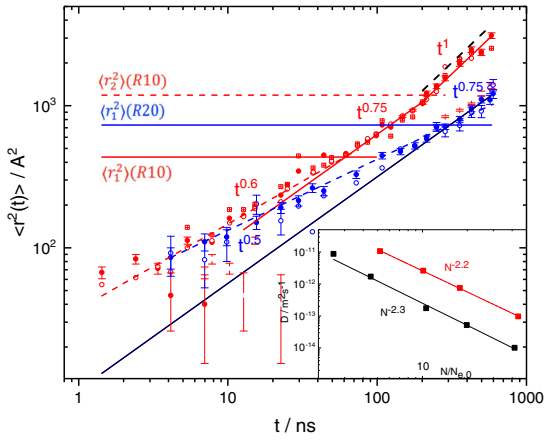

FIG. 1. Center of mass MSD as evaluated directly from the dynamic structure factor (see text) for $R10$ (red) and $R20$ (blue). Red crossed squares, open circles, and solid circles correspond to $q = 0.03$, 0.05, and 0.08 Å^{-1} for $R10$; blue filled and open circles relate to $q = 0.03$, 0.05 Å^{-1} for $R20$. The horizontal lines mark the different crossovers $\langle r_1^2\rangle$ and $\langle r_2^2\rangle$. Dashed black line shows the MSD extrapolated from PFG NMR diffusivity measured for $R10$ ring. Inset: PFG NMR results for the diffusion constants for rings in the melt (red squares) as a function of chain length. Black squares show diffusion coefficients for corresponding linear PEO melts. [23]

performed at the instrument IN15 of the Institute Laue-Langevin in Grenoble, France [24,25] and PHOENIX spectrometer of the MLZ in Munich, Germany [26]. Using four different neutron wavelengths $\lambda = 6$, 10, 13.5, and 17 Å a dynamic range $0.02 \le t \le 1000$ ns was achieved. The data were corrected for the scattering contribution of the deuterated matrix and the niobium container. Figures 2(a) and 2(b) show NSE spectra from the two large rings, $R40$ and $R100$. The solid lines are the result of the theoretical description that will be discussed in the following. Furthermore, in order to obtain the segmental self-correlation function $S_{\rm inc}(q,t) = \exp[-q^2\langle r^2(t)\rangle/6]$ that directly reveals the segmental MSD $\langle r^2(t)\rangle$ we studied the fully protonated $R100$ at $q = 0.12$ Å^{-1} and $q = 0.16$ Å^{-1}, respectively. The experiments were performed in order to clarify the important elements of polymer ring dynamics. Requirements were (i) The rings needed to be sufficiently large, in order to apply scaling approaches. (ii) The complexity of the ring dynamics demands to involve structural investigation by SANS [14] and long range diffusion measurements by PFG NMR.

The diffusion properties of polymer rings evidence three dynamic regimes [22], an early time subdiffusive motion with $D \sim t^{\alpha}(\alpha \le 0.65)$ which is followed by the established $D \sim t^{3/4}$ dynamics and finally by Fickian diffusion. The first two regimes are accessible by NSE at least for the smaller rings, the long range diffusion by PFG NMR. The com diffusion, respectively, the corresponding dynamic structure factor $S(q,t) = \exp[-q^2/6\langle r_{\rm com}^2(t)\rangle]$ reflects the time dependent center of mass mean-square-displacement $\langle r_{\rm com}^2(t)\rangle$ that involves the three dynamic regimes. The expression, realizing the proper crossover MSD's $\langle r_1^2\rangle$ and $\langle r_2^2\rangle$ is given in the Supplemental Material [27].

Figure 1 displays the $\langle r_{\rm com}^2(t)\rangle$ for $R10$ and $R20$ that are directly derived from the structure factor as $\langle r_{\rm com}^2(t)\rangle = -(6/q^2)\ln[S(q,t)]$ taken at sufficiently low q, such that internal modes do not contribute ($R10: q = 0.03$, 0.05, 0.08 Å^{-1}; $R20: q = 0.03$, 0.05 Å^{-1}). The $R10$ MSD clearly displays the two crossovers at $\langle r_1^2\rangle \cong 440$ Å^2 and $\langle r_2^2\rangle \cong 1200$ Å^2, while for $R20$ only the first crossover $\langle r_1^2\rangle \cong 740$ Å^2 is visible. The crossovers are marked by horizontal lines in Fig. 1. From simulations is known that $\langle r_2^2\rangle$ is expected to take place around $\langle r_2^2\rangle \cong 2, \ldots, 3R_g^2$. For $R10$ we have $\langle r_2^2\rangle/R_g^2 = 2.6$ in very good agreement with simulations. The first crossover $\langle r_1^2\rangle$ was already observed earlier [22] but remained unexplained. We find $\langle r_1^2\rangle(20\ {\rm K})/\langle r_1^2\rangle(10\ {\rm K}) = 1.68$ very close to the ratio of the two radii of gyration $27.8^2/21.4^2 = 1.69$ leading us to conjecture that $\langle r_1^2\rangle$ relates to the correlation hole effect as proposed for linear polymers by Guenza [28]. The correlation hole potential scales with R_g^2 and provokes com subdiffusivity characterized by an exponent α. For linear chains α decreases with increasing molecular weight [29]. With these results we scale $\langle r_1^2\rangle$ and $\langle r_2^2\rangle$ toward higher M_w as $\langle r_1^2\rangle, \langle r_2^2\rangle \sim R_g^2 \sim N^{0.78}$ [14]. The long range Fickian diffusion $D_{\rm com}$ was taken from NMR and corrected to the NSE regime (for further evaluation of the NSE data the NMR diffusion values were corrected by factor 1.3 visible in Fig. 1).

The internal ring motions are considered to evolve in two steps: At short time and distances the elementary loops perform Rouse dynamics with mode relaxation times $\tau_p \sim p^{-2}$, where p is the mode number. For larger distances and times the regime of loop relaxation follows. In terms of scaling theories, the mode spectrum has the form $\tau_p = \tau_2 p^{-\mu}$, where τ_2 is the first ring mode (only even modes are allowed) and μ the scaling exponent. Via a continuity condition at τ_e the two regimes are connected. In order to calculate the dynamic structure factor for internal ring dynamics $S_{\rm int}(q,t)$ we need to assume that the Rouse eigenvectors are an orthogonal basis also for the ring system. In their simulations on large PEO rings by Tsalikis *et al.* [17] have demonstrated this property. Then $S_{\rm int}(q,t)$ becomes [30,31]

$$S_{\rm int}(q,t) = \frac{1}{N}\sum_{i,j}\exp\left[\frac{(ql)^2}{6}\left(|i-j|\frac{N-|i-j|}{N}\right)^{2\nu_{ij}} - B_{i,j}(t)\right]$$

with

$$B_{i,j}(t) = \frac{2N^{2\nu_{ij}}(lq)^2}{3\pi^2}\sum_{p,\rm even}\frac{1}{p^2}\cos\left(\frac{p\pi[i-j]}{N}\right)[1-e^{-t\Gamma_p}] \quad (1)$$

ν_{ij} delineates the conformational crossover from Gaussian statistics at distances $|i-j| \leq N_{e,0}$ to compressed behavior $|i-j|^{2\nu}$ at larger distances. It is described by Fermi-type crossover functions taken from the SANS results: $\nu_{ij} = \theta_{|i-j|}\nu + (1-\theta_{|i-j|})\nu = 0.5$ with $\theta_n = \{1+\exp[(n-n_{\text{trans}})/n_{\text{width}}]\}^{-1}$, where $n_{\text{trans}} = N_{e,0}$. For the relaxation rate

$$\Gamma_p = \frac{[1-\theta_p]\pi^2 W l^4 p^2}{N^2 l^4} + \theta_p W \pi^2 \left(\frac{p}{p_{\min}}\right)^{\mu} \left(\frac{p_{\min}}{N}\right)^2 \qquad (2)$$

holds. $\theta_p = \{1+\exp[(p-p_{\min})/p_{\text{width}}]\}^{-1}$ is the crossover function in p with $p_{\min} = Z_{e,0}$ the number of elementary loops (Table I) and μ the spectral exponent. The basic Rouse rate $Wl^4 = 14890$ Å^4/ns is taken from NSE experiments on $M_w = 190$ kg/mol PEO melts also measured at the same temperature [11]. Including all the prior knowledge, we jointly fitted the spectra resulting from $R40$ and $R100$ varying only the spectral exponent μ and the exponents α_{R40} and α_{R100} that describe the first subdiffusive regime of the com diffusion [28]. All other parameters remained fixed. $n_{\text{trans}} = 45$ was taken from SANS [14]. Since the fits did not depend much on p_{width}, in order to establish a smooth crossover, we chose $p_{\text{width}} = 0.1 p_{\min}$. As Fig. 2 demonstrates the model leads to an excellent fit of all the spectra. For the slopes α_{Mw} in the first subdiffusive regime we obtain: $\alpha_{R10} = 0.65$; $\alpha_{R20} = 0.53$; $\alpha_{R40} = 0.54$; $\alpha_{R100} = 0.41$. Similar small exponents for the initial diffusion regime were also reported in recent MD simulations for PE rings [19]. For the scaling exponent the joint fit reveals $\mu = 2.4$ with a slowly growing flank toward higher μ (Fig. 2 and Supplemental Material [27]). Applying the same fitting procedure also to the large q regime of the $R10$ and $R20$ rings (see Supplemental Material [27]), we find $\mu(R10) = 5.0$ and $\mu(R20) = 2.5$; seemingly these smaller rings are not yet large enough to apply scaling considerations. We note that the fit results are very sensitive to the fractal exponents ν, thus it is essential to fix them to the values, which were obtained by SANS with high precision (better than 1%).

Discussing the results we first emphasize the overall goodness of fit: with only three fit parameters all spectra from $R40$ and $R100$ are excellently described. Let us now turn to the diffusion properties. The data analysis confirmed the three dynamic regimes of center of mass diffusion. In particular, the physical origin of the novel very short time regime seems to be clarified. Showing several attributes of the short time diffusion of linear chains in the melt, we conjecture that it results as a consequence of the correlation hole potential as first suggested by Guenza [28] for linear chains: (i) its dynamic regime extends to a range comparable to R_g^2 and it scales with R_g^2. This can be directly read out from the $R10$ and $R20$ $\langle r_{\text{com}}^2(t)\rangle$ and is corroborated by the excellent fits for $R40$ and $R100$; (ii) the exponents α decrease with increasing M_w, as was observed for linear PE

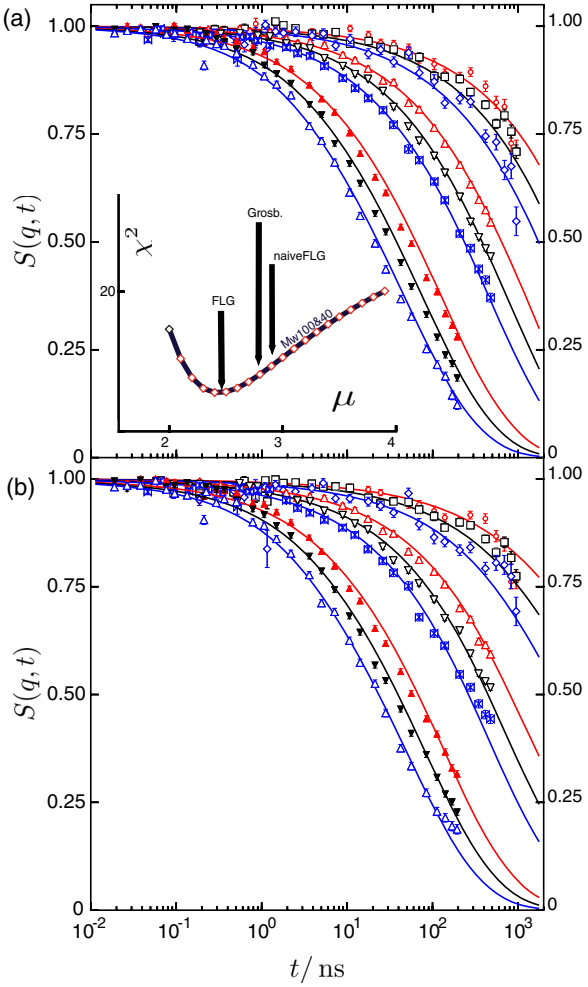

FIG. 2. NSE-spectra addressing the intraring pair correlation function (single chain dynamic structure factor) (a) from the $R40$ melt and (b) from the $R100$ melt; the q values from above are: 0.042, 0.049, 0.055, 0.069, 0.078, 0.086, 0.11, 0.12, 0.13 Å. The solid lines present the best fit using the scaling model (see text). The inset shows the sum of squares of a combined fit of NSE data for $R40$ and $R100$ as function of the spectral exponent μ. The arrows indicate the expectations from the discussed theory models.

melts [29]. On the basis of polymer integral equation theory recently Dell and Schweizer also emphasized the importance of correlation hole effects [18]. The M_w dependence of $D \sim N^{-2.2}$ agrees well with large scale MD simulations but is in disagreement with all the scaling models that predict diffusion exponents between about -1.6 (FLG) and -2 (DFLA, naive FLG). Seemingly the simple scaling argument $D \sim R_g^2/\tau_d \sim N^{0.78}/N^{2.4} \sim N^{-1.62}$ does not hold.

The concept of internal motion that takes place within two different dynamic regimes is well supported by our data. As the ring conformations already show, at short distances along the chain $|i-j| \leq N_{e,0} = 45$ the conformation is Gaussian and as in linear polymers Rouse dynamics is a valid model. Beyond this limit the conformation is compressed and loop dynamics is proposed

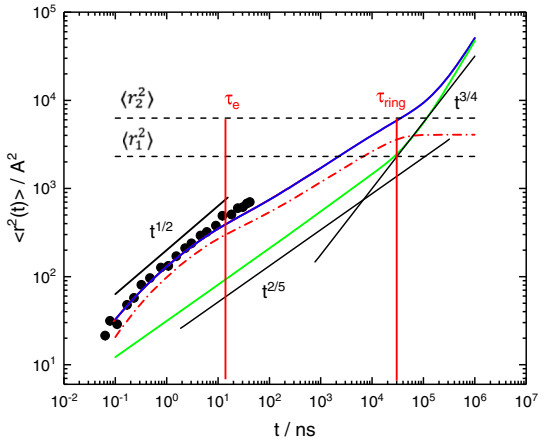

FIG. 3. Comparison of the segmental MSD for $R100$ ring, directly obtained from the self-correlation function (incoherent scattering) (symbols). Solid blue line presents MSD calculated from the best fit of the pair correlation function. Dash horizontal lines show the $\langle r_1^2 \rangle$ and $\langle r_2^2 \rangle$. The solid green line is the center of mass MSD and red dash-dotted line is the segmental MSD. The black solid lines demonstrate power laws, the vertical lines τ_e, τ_{ring} indicate the loop Rouse time and longest relaxation time of the ring, respectively. The figure extends the time range showing the predicted full dynamic regime based on the obtained fit parameters.

theoretically—the different scaling models distinguish themselves by different spectral exponents. The quality of the data description (i) shows that scaling models are well supported and (ii) the scaling exponent μ comes out close to the FLG prediction. However, inspecting sums of error χ^2 as a function of μ (see inset in Fig. 2 and Supplemental Material [27]) we find a rather broad minimum at $\mu = 2.4$ with slowly growing flank toward higher μ. The arrows in the inset indicate the scaling exponents predicted by the other models that lead to higher χ^2 but are not completely out of question. Nevertheless, our experiments agree best with Rubinstein's self-consistent FLG model for the internal ring dynamics even though the predictions for diffusion are not fulfilled. Finally, Fig. 3 compares the segmental MSD as calculated on the basis of the above described fit results (Fig. 2) with their direct measurement in terms of the self-correlation function. As may be seen, the direct measurement by incoherent scattering and the segmental MSD from the coherent structure factor perfectly agree with each other emphasizing the overall consistency of our approach (for more details, see Supplemental Material [27]). Furthermore, for $R100$ Fig. 3 extrapolates the fitting results to longer times such that the overall picture is evidenced.

In conclusion, combining results of SANS [14] and PFG NMR with NSE we could not only clarify the unique topology driven self-similar ring dynamics that is distinctly different to the dynamics of polymers featuring chain ends, but also distinguish between different scaling theories. Furthermore, an initial anomalous regime of center of mass diffusion could be related to the correlation hole effect.

The project has been funded by the Helmholtz Program "From Matter to Materials and Life" is gratefully acknowledged.

[1] P. G. de Gennes, Reptation of a polymer chain in the presence of fixed obstacles, J. Chem. Phys. **55**, 572 (1971).
[2] M. Doi and S. F. Edwards, *The Theory of Polymer Dynamics* (Clarendon Press Oxford, Oxford, 1986).
[3] J. D. Halverson, J. Smrek, K. Kremer, and A. Y. Grosberg, From a melt of rings to chromosome territories: The role of topological constraints in genome folding, Rep. Prog. Phys. **77**, 022601 (2014).
[4] M. Rubinstein, Dynamics of Ring Polymers in the Presence of Fixed Obstacles, Phys. Rev. Lett. **57**, 3023 (1986).
[5] S. P. Obukhov, M. Rubinstein, and T. Duke, Dynamics of a Ring Polymer in a Gel, Phys. Rev. Lett. **73**, 1263 (1994).
[6] A. Y. Grosberg, Annealed lattice animal model and Flory theory for the melt of non-concatenated rings: Towards the physics of crumpling, Soft Matter **10**, 560 (2014).
[7] T. Ge, S. Panyukov, and M. Rubinstein, Self-similar conformations and dynamics in entangled melts and solutions of nonconcatenated ring polymers, Macromolecules **49**, 708 (2016).
[8] T. A. Kavassalis and J. Noolandi, Entanglement scaling in polymer melts and solutions, Macromolecules **22**, 2709 (1989).
[9] L. J. Fetters, D. J. Lohse, D. Richter, T. A. Witten, and A. Zirkel, Connection between polymer molecular weight, density, chain dimensions, and melt viscoelastic properties, Macromolecules **27**, 4639 (1994).
[10] The packing model states that in order to form an entanglement a number of about 20 uninterrupted chains need to pass through the volume spanned by an entanglement strand resulting in the condition $O_{\mathrm{KN}} \cong l^3 N_e^{1/2}/v \approx 20$.
[11] B. J. Gold, W. Pyckhout-Hintzen, A. Wischnewski, A. Radulescu, M. Monkenbusch, J. Allgaier, I. Hoffmann, D. Parisi, D. Vlassopoulos, and D. Richter, Direct Assessment of Tube Dilation in Entangled Polymers, Phys. Rev. Lett. **122**, 088001 (2019).
[12] P. Malo de Molina, A. Alegría, J. Allgaier, M. Kruteva, I. Hoffmann, S. Prévost, M. Monkenbusch, D. Richter, A. Arbe, and J. Colmenero, Direct Observation of Dynamic Tube Dilation in Entangled Polymer Blends: A Combination of Neutron Scattering and Dielectric Techniques, Phys. Rev. Lett. **123**, 187802 (2019).
[13] J. Smrek and A. Y. Grosberg, Understanding the dynamics of rings in the melt in terms of the annealed tree model, J. Phys. Condens. Matter **27**, 064117 (2015).
[14] M. Kruteva, J. Allgaier, M. Monkenbusch, L. Porcar, and D. Richter, Self-similar polymer ring conformations based on elementary loops: A direct observation by SANS, ACS Macro Lett. **9**, 507 (2020).
[15] J. D. Halverson, W. B. Lee, G. S. Grest, A. Y. Grosberg, and K. Kremer, Molecular dynamics simulation study of nonconcatenated ring polymers in a melt. II. Dynamics, J. Chem. Phys. **134**, 204905 (2011).

[16] J. D. Halverson, G. S. Grest, A. Y. Grosberg, and K. Kremer, Rheology of Ring Polymer Melts: From Linear Contaminants to Ring-Linear Blends, Phys. Rev. Lett. **108**, 038301 (2012).

[17] D. G. Tsalikis, T. Koukoulas, V. G. Mavrantzas, R. Pasquino, D. Vlassopoulos, W. Pyckhout-Hintzen, A. Wischnewski, M. Monkenbusch, and D. Richter, Microscopic structure, conformation, and dynamics of ring and linear poly(ethylene oxide) melts from detailed atomistic molecular dynamics simulations: Dependence on chain length and direct comparison with experimental data, , Macromolecules **50**, 2565 (2017).

[18] Z. E. Dell and K. S. Schweizer, Intermolecular structural correlations in model globular and unconcatenated ring polymer liquids, Soft Matter **14**, 9132 (2018).

[19] C. P. J. Wong and P. Choi, On the diffusivity of ring polymers, Soft Matter **16**, 2350 (2020).

[20] K. Hur, C. Jeong, R. G. Winkler, N. Lacevic, R. H. Gee, and D. Y. Yoon, Chain dynamics of ring and linear polyethylene melts from molecular dynamics simulations, Macromolecules **44**, 2311 (2011).

[21] S. T. Milner and J. D. Newhall, Stress Relaxation in Entangled Melts of Unlinked Ring Polymers, Phys. Rev. Lett. **105**, 208302 (2010).

[22] S. Gooßen, A. R. Brás, M. Krutyeva, M. Sharp, P. Falus, A. Feoktystov, U. Gasser, W. Pyckhout-Hintzen, A. Wischnewski, and D. Richter, Molecular Scale Dynamics of Large Ring Polymers, Phys. Rev. Lett. **113**, 168302 (2014).

[23] M. Kruteva, J. Allgaier, and D. Richter, Direct observation of two distinct diffusive modes for polymer rings in linear polymer matrices by pulsed field gradient (PFG) NMR, Macromolecules **50**, 9482 (2017).

[24] M. Kruteva, J. Allgaier, I. Grillo, I. Hoffmann, L. Porcar, D. Richter, and R. Schweins, Self similar dynamics of ring polymers, Institut Laue-Langevin (ILL) (2019), https://doi.org/10.5291/ILL-DATA.9-11-1895.

[25] B. Farago, P. Falus, I. Hoffmann, M. Gradzielski, F. Thomas, and C. Gomez, The in15 upgrade, Neutron News **26**, 15 (2015).

[26] S. Pasini, O. Holderer, T. Kozielewski, D. Richter, and M. Monkenbusch, J-NSE-Phoenix, a neutron spin-echo spectrometer with optimized superconducting precession coils at the MLZ in garching, Rev. Sci. Instrum. **90**, 043107 (2019).

[27] See Supplemental Material at http://link.aps.org/supplemental/10.1103/PhysRevLett.125.238004 for the expressions describing centre-of-mass diffusion and segmental mean squared displacement, fitting results for the lower molecular weight rings, comparison of the sum of squares deviation for the different scaling models in terms of the spectral index μ.

[28] M. Guenza, Cooperative Dynamics in Unentangled Polymer Fluids, Phys. Rev. Lett. **88**, 025901 (2001).

[29] M. Zamponi, A. Weschnewski, M. Monkenbusch, L. Willner, D. Richter, P. Falus, B. Farago, and M. G. Guenza, Cooperative dynamics in homopolymer melts: A comparison of theoretical predictions with neutron spin echo experiments, J. Phys. Chem. B **112**, 16220 (2008).

[30] G. Tsolou, N. Stratikis, C. Baig, P. S. Stephanou, and V. G. Mavrantzas, Melt structure and dynamics of unentangled polyethylene rings: Rouse theory atomistic molecular dynamics simulation, and comparison with the linear analogues, Macromolecules **43**, 10692 (2010).

[31] A. Bensafi, U. Maschke, and M. Benmouna, Cyclic polymers in good solvents, Polym. Int. **49**, 175 (2000).